

ACCEPTED MANUSCRIPT • OPEN ACCESS

Investigation of the role of hydrogen molecules in 1D simulation of divertor detachment

To cite this article before publication: Yulin Zhou *et al* 2022 *Plasma Phys. Control. Fusion* in press <https://doi.org/10.1088/1361-6587/ac6827>

Manuscript version: Accepted Manuscript

Accepted Manuscript is “the version of the article accepted for publication including all changes made as a result of the peer review process, and which may also include the addition to the article by IOP Publishing of a header, an article ID, a cover sheet and/or an ‘Accepted Manuscript’ watermark, but excluding any other editing, typesetting or other changes made by IOP Publishing and/or its licensors”

This Accepted Manuscript is © 2022 The Author(s). Published by IOP Publishing Ltd..

As the Version of Record of this article is going to be / has been published on a gold open access basis under a CC BY 3.0 licence, this Accepted Manuscript is available for reuse under a CC BY 3.0 licence immediately.

Everyone is permitted to use all or part of the original content in this article, provided that they adhere to all the terms of the licence <https://creativecommons.org/licenses/by/3.0>

Although reasonable endeavours have been taken to obtain all necessary permissions from third parties to include their copyrighted content within this article, their full citation and copyright line may not be present in this Accepted Manuscript version. Before using any content from this article, please refer to the Version of Record on IOPscience once published for full citation and copyright details, as permissions may be required. All third party content is fully copyright protected and is not published on a gold open access basis under a CC BY licence, unless that is specifically stated in the figure caption in the Version of Record.

View the [article online](#) for updates and enhancements.

Investigation of the role of hydrogen molecules in 1D simulation of divertor detachment

Yulin Zhou^{1,3}, Benjamin Dudson^{1,4}, Fulvio Militello², Kevin Verhaegh² and Omkar Myatra²

¹ York Plasma Institute, Department of Physics, University of York, YO10 5DQ, UK

² United Kingdom Atomic Energy Authority, Culham Centre for Fusion Energy, Culham Science Centre, Abingdon, Oxon, OX14 3DB, United Kingdom

³Southwestern Institute of Physics, Chengdu 610041, China

⁴Lawrence Livermore National Laboratory, 7000 East Ave, Livermore, CA 94550, USA

Abstract

The role of neutral and charged hydrogenic molecules in detached regimes of tokamak plasmas is investigated using a simplified 1D numerical model. Using MAST Upgrade like conditions, simulations are implemented to study the rollover of target flux Γ in upstream density scan. It is found that if H_2 and H_2^+ are considered in simulations a lower target temperature and a larger upstream density will be required to trigger divertor detachment under the same input power and particle flux, and the critical detachment threshold (the critical ratio of upstream static pressure to the power entering the recycling region) is found to be $\frac{p_{up}}{P_{recl}} \sim 8.1 \text{ N/MW}$ at rollover. Molecule-plasma interactions are found to be as crucial as atom-plasma interactions during divertor detachment, both of which account for the majority of plasma momentum loss in the cases studied here. Further analysis of the momentum loss decomposition shows molecule-plasma elastic collisions dominate molecule-plasma interactions, while molecular charge exchange cannot effectively reduce plasma momentum. In terms of H_{alpha} emission, a strong rise of H_{alpha} signal is found to be due to molecular excitation channels when the upstream density further increases after rollover.

Keywords: tokamak, divertor detachment, molecules, plasma momentum loss, H_{alpha} emission, SD1D

A. Introduction

Seeding impurities and increasing the upstream density are the two most widely used approaches to reach the detached divertor regime [1][2]. In the first detachment regime, the divertor volume is cooled down mainly due to the radiation from impurities, which are generated by plasma-material interactions (e.g. sputtering from plasma facing materials, leading to the release of C , W) [3] or extrinsic impurity seeding (e.g. N_2 , Ne) [4]. During a density ramp discharge, molecular hydrogen H_2 may be injected through gas puffing, raising the density in the core and leading to an increasing upstream density, which is able to cause a lower target plasma temperature according to the two point model (TPM)[2]. The increasing upstream density also enhances recycling at the target, which results in an increased neutral density that interacts with the plasma flux moving towards the target and further cools it. Despite general consensus on the importance of impurities and neutral particles on divertor detachment, uncertainties remain in the details of how the molecular species (H_2 , H_2^+ and H_3^+) influence divertor physics before and after flux rollover is achieved, and how these in turn affect the conditions to achieve divertor detachment [5][6]. For example, the effects of molecular processes (e.g. molecular charge exchange, molecular activated recombination (MAR), molecular assisted ionization (MAI)) on the momentum and power loss in the

divertor volume [7][8], the effect of plasma recycling with different wall and target materials [9] [10], and the importance of hydrogenic radiation [11] in different detachment discharge regimes are all active areas of research. These studies are crucial for understanding the atomic and molecular physics in the divertor volume, and will be helpful to better control divertor detachment in experiment. Sophisticated 2D edge plasma transport codes, e.g. SOLPS, EDGE2D, SOLEDGE2D [12][13][14], have been widely used for studying edge plasma phenomena e.g. divertor detachment, but they are often too complex for easy interpretation of the physics involved. Simplified analytic [2][15] and 1D computational model (e.g. [16][17][18][19]) can provide more details of the underlying processes in the edge plasma, despite some simplifications and omissions, such as simplified geometry and treatment of cross field transport. Therefore, making reasonable assumptions is crucial in 1D simulations. This paper aims to explore the dynamics of molecular species and their effects on the detachment process with a BOUT++ module named SD1D[16] (section B.1). SD1D is a time-dependent code and can be used to investigate the importance of power and momentum loss to the detachment process, the profile variation in different detachment discharge regimes, feedback control of detachment, and the dynamics of different particle species during the detachment process [16]. In [16] only the dynamics of plasma and neutral atoms were included in the SD1D model. To investigate the effects of molecular species, we have upgraded the SD1D model: the dynamics of H_2 and H_2^+ , the collisional reactions related to these molecular species, and the hydrogen radiation from excited atoms after molecular break-up involving (H_2, H^-, H_2^+) have been added to the physical model (section B.2). The reaction rate coefficients and hydrogen radiation emissivity used in the upgraded SD1D are shown in section C. These coefficients are calculated by the data from the EIRENE-Amjuel database [20], another improvement over the original SD1D code used in [16]. With the upgraded SD1D, we primarily use an upstream density scan to analyse the cases with and without carbon impurity in MAST Upgrade conditions, the variations of plasma ion flux to the target in different recycling conditions, the critical detachment threshold, the importance of molecular species on plasma momentum loss, and the various contributors to the H_{alpha} emission as shown in section D.

B. The SD1D model

1. The physical model of old SD1D version

SD1D uses a 1D time dependent fluid model [2][18], which evolves the plasma density n , parallel momentum density $m_H + nv_{\parallel}$ and static pressure $p = 2enT$. The plasma equations are shown below [16]:

$$\frac{\partial n}{\partial t} = -\nabla \cdot [\mathbf{b}v_{\parallel}n] + S_n - S \quad (1a)$$

$$\frac{\partial}{\partial t} \left(\frac{3}{2} p \right) = -\nabla \cdot \mathbf{q}_e + v_{\parallel} \partial_{\parallel} p + S_E - E - R \quad (1b)$$

$$\frac{\partial}{\partial t} (m_H + nv_{\parallel}) = -\nabla \cdot [m_H + nv_{\parallel} \mathbf{b}v_{\parallel}] - \partial_{\parallel} p - F \quad (1c)$$

Where $\partial_{\parallel} = \mathbf{b} \cdot \nabla$, the heat flux is $\mathbf{q}_e = \frac{5}{2} p \mathbf{b}v_{\parallel} - \kappa_{\parallel} \partial_{\parallel} T_e$, and the Braginskii thermal conduction coefficient is $\kappa = \kappa_0 T^{\frac{5}{2}}$. The constant $\kappa_0 = 2293.8 [MW/m^2/eV^{\frac{5}{2}}]$ and m_{H^+} is the mass of the main ions. v_{\parallel} is the parallel velocity of the main ions. The ion and electron temperatures are assumed to be equal and isotropic: $T = T_e = T_{H^+}$, while their densities are equal as well: $n_e = n_{H^+}$. In eq.1a, S_n is the external particle source evolved by a proportional-integral (PI) feedback controller. S shows the particle sources and sinks caused by collisional reactions like ionisation and recombination. In eq.1b, S_E represents an external source of power that keeps injecting energy with a fixed rate into a volume above X-point; E represents energy exchange due to plasma-neutral interactions; R is radiation power generated by hydrogen atom radiation and impurity radiation. The particle sources and sinks (S), friction force (F), and energy sources and sinks (E and R) caused by collisional reactions can be found in the Appendix (section F.1).

The equations of atom density n_H , atom parallel momentum $n_H v_{\parallel H}$ and atom static pressure $n_H T_H$ are similar to eq.1a – eq.1c. Since the magnetic field is unable to confine the neutrals, the atoms can be transported across the magnetic field and spread upstream. To model this process, SD1D gives an effective parallel velocity to atoms which is the sum of a parallel flow and parallel projection of a perpendicular diffusion [16]: $v_H = v_{\parallel, H} - (\frac{B_\phi}{B_\theta})^2 \frac{\partial_{\parallel} p_H}{v}$, where total atom collision frequency v is calculated by the sum of charge exchange rate, ionisation rate and neutral-neutral collision rate and the cross-field neutral diffusion multiplier (field-line pitch) $(\frac{B_\phi}{B_\theta})^2$ is equal to 10 in the simulations shown here.

Only atomic species were included in the original SD1D neutral model, while volumetric processes involving molecular species were not directly calculated, being only included indirectly in the effective radiation rate. As discussed in section A, molecules can be a crucial part of divertor plasma dynamics due to strong interactions with other particle species, thus it is necessary to create a molecular model in SD1D. Including density, energy and momentum equations for molecular species is also beneficial to model the profile evolution self-consistently. An impurity model ‘atomic++coronal’, has been added to in SD1D [21]. It is able to provide impurity radiation power (i.e. carbon) with a fixed impurity fraction, through fetching and using data from ADAS database [22].

Bohm boundary conditions are used at the target, where the parallel plasma velocity $v_{\parallel} \geq c_s$, where the plasma sound speed is $c_s = \sqrt{\frac{2 \times T}{m_{H^+}}}$. The plasma density and pressure boundaries are ‘free’, so that they are extrapolated into the boundary. The temperature gradient at the sheath entrance is set to zero, replacing the heat conduction with an energy flux corresponding to a sheath heat transmission of $q = \gamma n T c_s$ [16], where the sheath transmission coefficient γ is equal to 6. For recycling processes at the target, here the recycling fraction of ion flux to the target is set to $f_{recl} = \frac{\Gamma_{recl}}{\Gamma_{ion}^t} = 0.99$, so that 99% of the plasma ion flux to the target Γ_{ion}^t is recycled and becomes the neutral flux Γ_{recl} (made up of atoms and molecules) in the final grid point at the target [16].

2. SD1D upgrades

In the previous version of SD1D, only atomic collisional and radiative reactions were included, while molecular processes were included only in the collisional-radiative model used to derive the effective rates. To better investigate the physics of divertor detachment, an important upgrade of the SD1D model was carried out by adding a molecule model, including an explicitly evolved hydrogen molecule model labelled ‘ H_2 ’ and a charged molecule model labelled ‘ H_2^+ ’. Similar to the atom model, equations of molecule density n_{H_2} (eq.2a), pressure p_{H_2} (eq.2b) and parallel momentum $n_{H_2} v_{\parallel H_2}$ (eq.2c) are used in the form of equations (eq.1a – eq.1c). The terms of the sources, sinks (S_{H_2} and E_{H_2}) and friction force (F_{H_2}) are generated by the collisional reactions listed in Table 1, including non-dissociative ionisation, dissociation, molecular charge exchange and molecular activated recombination (MAR) via H^- (see section F.1). In eq.2d, \mathbf{q}_{H_2} is the energy convection flux of neutral molecules. Following the effective parallel velocity to atoms in section B.1, a parallel velocity v_{H_2} similar to the v_H in section B.1 is given to molecules in the current SD1D implementation, with the cross-field neutral diffusion $(\frac{B_\phi}{B_\theta})^2 = 10$. The total molecule collision frequency is calculated by the sum of molecular charge exchange rate, non-dissociative ionisation rate and neutral-neutral collision rate.

The model used here contains two neutral species, atoms and molecules. According to experimental observations in divertors, both atoms and molecules are important plasma recycling channels, their relative ratio depending on the target material (e.g. carbon and

tungsten)[9][10]. In section D, a comparison is made to study divertor detachment with different proportion of recycled atoms and molecules.

$$\frac{\partial n_{H_2}}{\partial t} = -\nabla \cdot [\mathbf{b} v_{\parallel, H_2} n_{H_2}] - S_{H_2} \quad (2a)$$

$$\frac{\partial}{\partial t} \left(\frac{3}{2} p_{H_2} \right) = -\nabla \cdot \mathbf{q}_{H_2} + v_{\parallel, H_2} \partial_{\parallel} p_{H_2} - E_{H_2} \quad (2b)$$

$$\frac{\partial}{\partial t} (m_{H_2} n_{H_2} v_{\parallel, H_2}) = -\nabla \cdot [m_{H_2} n_{H_2} \mathbf{b} v_{\parallel, H_2}] + \partial_{\parallel} p_{H_2} - F_{H_2} \quad (2c)$$

$$\mathbf{q}_{H_2} = \frac{5}{2} p_{H_2} \mathbf{b} v_{\parallel, H_2} \quad (2d)$$

Consistently with the atomic and neutral molecules equations, a similar set of three equations for the charged molecule H_2^+ is also added in SD1D: the sources, sinks ($S_{H_2^+}$ and $E_{H_2^+}$) and friction force ($F_{H_2^+}$) in the equations of density $n_{H_2^+}$, pressure $p_{H_2^+}$ and momentum $n_{H_2^+} v_{\parallel, H_2^+}$ are determined by dissociative excitation, molecular ionisation, dissociative ionisation, dissociative recombination and molecular charge exchange shown in Table 1 (reaction 4, 6, 7, 8 and 9). As discussed in section B.1, Bohm boundary conditions are also used for H_2^+ at the

target, where the parallel plasma velocity $v_{\parallel, H_2^+} \geq c_{s, H_2^+}$, where $c_{s, H_2^+} = \sqrt{\frac{2 \times T_{H_2^+}}{m_{H_2^+}}}$. The density and pressure boundaries of H_2 and H_2^+ are ‘free’. The temperature gradient of H_2^+ at the sheath entrance is also zero, and the energy flux is related to a sheath heat transmission of $q_{H_2^+} = \gamma n_{H_2^+} T_{H_2^+} c_{s, H_2^+}$, where $\gamma=6$.

In order to compare the simulations of the upgraded SD1D to the previous work, the assumptions (e.g. $T_{H^+} = T_e$ and $n_{H^+} = n_e$) made in the previous version [16] are still used in this work. Although another ion species H_2^+ is considered in the upgraded code, its density $n_{H_2^+}$ is small ($\frac{N_{H_2^+}}{N_{H_2^+} + N_{H^+}} < 0.022$ when $T_e < 7\text{eV}$) and is only distributed in a very narrow area in front of the target (see figure D.3). Therefore, a trace assumption is applied for H_2^+ , which means $n_{H_2^+}$ does not enter into the quasineutrality assumption $n_{H^+} = n_e$. Since the paper focuses on cases of divertor detachment (related to low target temperatures), it is expected that the trace assumption will not affect the main results in the paper (e.g. the rollover of target flux, momentum loss and photon emission during detachment). But in some attached cases T_e in the recycling region is high (e.g. $T_e > 15\text{eV}$), such that $\frac{N_{H_2^+}}{N_{H_2^+} + N_{H^+}}$ can be over 7% and $\frac{N_{H_2^+}}{N_{H_2^+} + N_{H^+}}$ will be no longer negligible in front of the target. So if future studies focus on the cases with high target temperatures, the trace assumption on H_2^+ may not be suitable, but require changes to the electron equations.

The main ions and electrons have their own density and pressure equations (with different energy flux, different sources and different sinks). If it is assumed that $T_e \neq T_{H^+}$ and $n_e \neq n_{H^+}$, their densities and pressure can be calculated separately. It will be important for the cases with significant quantities of impurities in future studies.

Table 1. List of collisional reactions (black) in the atom model and the reactions (blue) in the molecule model

Index	Reactions	Reaction types
1	$e + H \rightarrow 2e + H^+$	Ionization
2	$H^+ + H \rightarrow H + H^+$	Charge exchange
3	$H^+ + e \rightarrow H$	Electron-ion Recombination
4	$e + H_2 \rightarrow 2e + H_2^+$	Non-dissociative Ionization

5	$e + H_2 \rightarrow e + H + H$	Dissociation
6	$H^+ + H_2 \rightarrow H_2^+ + H$	Molecular charge exchange
7	$e + H_2^+ \rightarrow e + H^+ + H$	Dissociative excitation
8	$e + H_2^+ \rightarrow 2e + H^+ + H^+$	Dissociative ionization
9	$e + H_2^+ \rightarrow H + H$	Dissociative recombination
10	$H^+ + H_2 + e \rightarrow H + H + H$	MAR via H^-

In the original SD1D model, semi-analytic approximations [23][24] were used to calculate hydrogenic rates, such as rate coefficients of atom-plasma interactions and hydrogen emissivity. According to those approximations, however, the reaction rate coefficients for ionisation and charge exchange only depend on the electron temperature T_e (electron-ion recombination rates included density variation). This, however, was not very precise since rate coefficients have a n_e dependence as well, which is particularly strong for the rate coefficient of electron-ion recombination, ionisation, and dissociative recombination.

Taking into account the density dependence of the plasma-neutral interactions is important because the electron density in the divertor can significantly change depending on the operating conditions and is sensitive to the variation of the upstream density, heat and particle flux. When divertor detachment is triggered by increasing the upstream density, the peak electron density in divertor will be several times larger than during attached conditions, while the divertor electron density can decrease when the divertor is fully detached. Thus, it is essential to consider electron density variation in the calculation of rate coefficients and hydrogenic radiation. To solve this issue, the ‘Amjuel’ database is now been used in SD1D. Amjuel provides double polynomial fitting expression as a function of electron temperature and density to calculate rate coefficients of electron-atom, electron-ion and electron-molecule interactions (i.e. ionisation, dissociation, recombination and the reactions related to molecule) [20]. For the ion-atom, ion-molecule interactions (i.e. charge exchange), its double polynomial expression is a function of energies of the two collided particles [20].

Besides collisional reactions, the hydrogen atom radiation caused by atom-plasma or molecule-plasma interactions is also crucial for divertor physics [11]. It contributes a significant energy loss from the plasma in divertor volume, and greatly affects the target flux in terms of particle and power balance. The previous SD1D version already considered hydrogen electron-impact excitation and electron-ion recombination, but its hydrogen atom emissivity was an empirical function of T_e , derived from fits to collisional-radiative models. According to the discussion about rate coefficient fitting functions above, it is more precise and reliable to associate the emissivity with both T_e and n_e . Furthermore, radiation from hydrogen atoms that are excited after molecular break-up was not included in the old version. Here, the hydrogen emissivity as a function of T_e and n_e can be modelled by the population coefficients from Amjuel. According to the collisional and radiative models [25], there are 6 channels to generate excited hydrogen atoms. Direct electron-impact excitation (via H) and electron-ion recombination (via H^+) are atomic excitation channels. Dissociation (via H_2), dissociative recombination (via H_2^+ and H_3^+) and mutual neutralization (via H^-) are molecular excitation channels, since they generate excited atoms after molecular break-up. Just as the channel’s names imply, the radiative reactions always happen together with the corresponding collisional reactions.

The radiation power produced by every channels is obtained by the following steps. I_{pq} is the emission intensity from state ‘p’ to ‘q’ and defined as

$$I_{pq} = n_e N_0 \chi_{pq}^{eff}, \quad (3)$$

$$\chi_{pq}^{eff} = R_{0p} A_{pq}, \quad (4)$$

$$R_{0p} = \frac{N_p}{n_e N_0}, \quad (5)$$

where χ_{pq}^{eff} is effective emission rate coefficient and R_{0p} represents the population coefficient of the excited hydrogen atom in state ‘p’ [20]; A_{pq} is the Einstein coefficient or rate of

transmitting from state 'p' to 'q' [26]; N_0 is the density of the reacting species which collides with electrons to generate atoms in the excited state 'p' (e.g for direct electron-impact excitation N_0 represents the density of hydrogen atom). From eq. (3-5), we can get the emission intensity of the excited atom from state 'p' to 'q' in eq. 6.

$$I_{pq} = n_e N_0 \chi_{pq}^{eff} = n_e N_0 \times \frac{N_p}{n_e N_0} \times A_{pq} = N_p A_{pq} \quad (6)$$

Then multiplying I_{pq} by the energy gap between any two states E_{pq} [26], the radiation power density (W/m^3) by the excited atoms in a certain state 'p' is obtained by eq. 7.

$$\varepsilon_{rad,pq} = E_{pq} \times I_{pq} \quad (7)$$

Through summing the radiation power density over energy level transitions (only Lyman series of $p=2-6 \rightarrow 1$ is considered), the radiation power density of an excitation channel can be written as [27]:

$$\varepsilon_{rad,p \rightarrow 1}^{channel} = \sum_{p=2}^6 E_{p \rightarrow 1} N_p A_{p \rightarrow 1} \quad (8)$$

Repeat the calculation for all the 6 excitation channels, and we can get the total hydrogen atom radiation power per volume (e.g in the unit W/m^3) by summing the radiation power density of all channels.

The dynamics of H_3^+ and H^- are not considered in the upgraded SD1D due to their negligible density and limited contribution to the energy loss in experiment [11][28]. According to equation 8, it is also found that the radiated power due to H_3^+ and H^- channels is small. In order to study the H_{alpha} photon emission, the hydrogen atom radiation via H^- is still added in the current SD1D model by using a fraction of H^- density ($\frac{n_{H^-}}{n_{H_2}}$) as a function of T_e and n_e [20].

In the next section, the rate coefficients of collisional reactions and the hydrogen emissivity of five excitation channels (except H_3^+) will be discussed.

C. Analysis of collisional and radiative reactions with open databases

A number of collisional and radiative reactions occur in the tokamak edge and divertor, and greatly affect transport processes. Public databases provide the required molecular reaction rate coefficients, including EIRENE and ADAS [20][22]. Even though ADAS is now one of the most reliable databases for studying atomic processes, it does not contain any data related to molecular species. We are employing it to provide impurity radiation in the SD1D simulations, by using the impurity model '[atomic++coronal](#)' [21][22]. The EIRENE code is widely used in fusion-related numerical studies, i.e. SOLPS[29], EDGE2D[13] and EMC3[30]. Amjuel[20] and Hydhel[31] databases contain extensive information on atomic and molecular reactions which are contained in EIRENE including cross-sections, rate coefficients and population coefficients. While the reaction rate coefficients of ionisation, recombination, charge exchange, dissociation etc, are just a function of T_e in Hydhel, Amjuel presents a double polynomial fitting function of both T_e and n_e . Allowing for n_e variations, has a profound effect on the calculated rates. To further compare the two databases, the rate coefficients of the plasma-neutral collisional reactions are plotted and compared in the Appendix (section F.2). In the upgraded SD1D simulations, all the reaction rate coefficients are obtained from Amjuel and the population coefficients in Amjuel are applied to calculate hydrogen emissivity (in section B.2) [20].

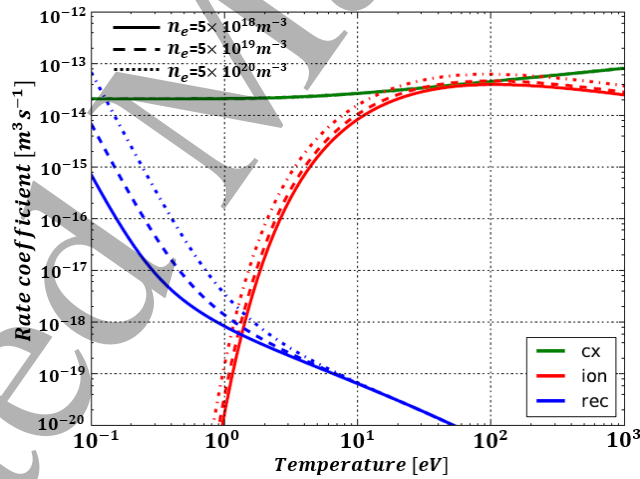
1. The rate coefficients of hydrogen atomic and molecular reactions

The rate coefficients for the reactions shown in Table 1 for both hydrogen atom and molecule are shown in figure C.1-C.3 as a function of electron temperature T_e . Each reaction has three curves, which represents the rate coefficient at three different electron densities: $n_e =$

1
 2
 3 $5 \times 10^{18}/m^3$, $n_e = 5 \times 10^{19}/m^3$ and $n_e = 5 \times 10^{20}/m^3$. In figure C.1, the ionisation, charge
 4 exchange and recombination rate coefficients show the basic processes occurring during
 5 divertor detachment: (1) ionisation and charge exchange are the dominant atomic processes at
 6 higher T_e ; (2) once T_e goes down ($T_e < 10\text{eV}$), the ionisation rate coefficient drops, and charge
 7 exchange becomes the most significant atomic process; (3) recombination becomes more
 8 significant at $T_e < 1\text{eV}$. The effective volume ionisation and recombination rates, which are
 9 important for describing detached plasma, are affected by both the rate coefficients. In figure
 10 C.2, the rate coefficient curves shows non-dissociative ionisation is the main molecule sink at
 11 high temperatures, with electron-impact dissociation contributing more when $T_e \sim 10\text{eV}$. Once
 12 $T_e < 10\text{eV}$, both dissociation rate coefficient and non-dissociative ionisation rate coefficient
 13 dramatically decrease, and molecular charge exchange gradually becomes the main molecule
 14 sink ($T_e \sim 2.0\text{eV}$).
 15

16 H_2^+ is an important product from molecule collisional reactions. There are three channels for
 17 the dissociation of H_2^+ : dissociative excitation ($e + H_2^+ \rightarrow e + H^+ + H$), dissociative
 18 ionisation ($e + H_2^+ \rightarrow 2e + H^+ + H^+$) and dissociative recombination ($e + H_2^+ \rightarrow e + H + H$). Through comparing the rate coefficients in figure C.3 to the coefficients of non-dissociative
 19 ionization and molecular charge exchange in figure C.2, the rate at which H_2^+ is dissociated is
 20 generally larger than the rate at which H_2^+ is produced, therefore the density of H_2^+ is always
 21 small. The density ratio $\frac{n_{H_2^+}}{n_{H_2}}$ is about 0.01 in the electron temperature range $1\text{eV} < T_e < 10\text{eV}$.
 22

23 During detachment with fueling in the divertor, molecules can be injected into the divertor
 24 volume by localized gas puffing, but it is typically recycling the main process that generates
 25 molecules near the target. As the molecular density increases, more H_2^+ will be produced and
 26 thus the H_2^+ collisional reactions will become more important. As a result, in such conditions
 27 this charged molecule plays a bigger role in the dynamics of detachment.
 28



46
 47 *Figure C.1: Hydrogen atom effective ionisation, charge exchange and recombination rate*
 48 *coefficients as a function of electron temperature for electron density $n_e = 5 \times 10^{18}/m^3$,*
 49 *$n_e = 5 \times 10^{19}/m^3$ and $n_e = 5 \times 10^{20}/m^3$.*

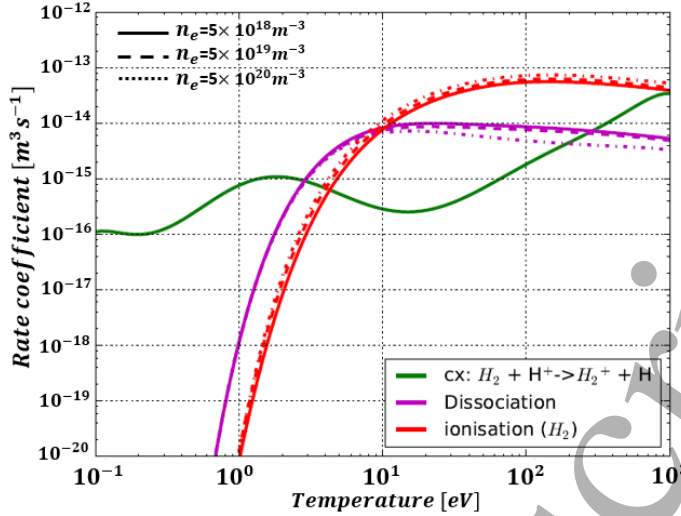


Figure C.2: Hydrogen molecule effective charge exchange, dissociation, and non dissociative ionisation rate coefficients as a function of electron temperature for electron density $n_e = 5 \times 10^{18}/m^3$, $n_e = 5 \times 10^{19}/m^3$ and $n_e = 5 \times 10^{20}/m^3$.

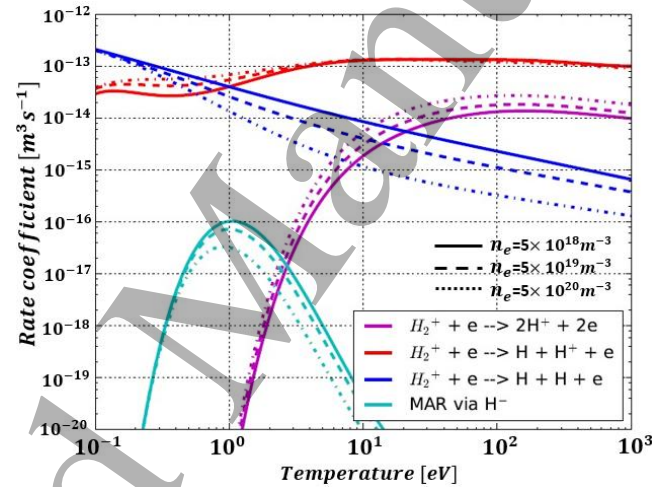


Figure C.3: Rate coefficients of effective dissociative ionisation (purple), dissociative excitation (red), dissociative recombination (blue) and molecular activated recombination (MAR) via H^- , as a function of electron temperature for electron density $n = 5 \times 10^{18}/m^3$, $n_e = 5 \times 10^{19}/m^3$ and $n_e = 5 \times 10^{20}/m^3$.

2. Analysis of hydrogen atomic and molecular excitations with Amjuel database

The emissivity $L = \epsilon_{rad,pq}/n_e N_0$ (in $\text{erg} * \text{cm}^3/\text{s}$) corresponding to the low- n and medium- n Lyman lines (e.g $n=2-6 \rightarrow 1$) are shown in figure C.4 for direct electron-impact excitation (via H) and recombination (via H^+), dissociation (via H_2), dissociative recombination (via H_2^+) and mutual neutralization (via H^-) at three different electron densities. As mentioned in section B.2, the radiative reactions always happen together with the corresponding collisional reactions. Qualitatively, the curves of the ionisation rate coefficient and recombination rate coefficient shown in figure C.1 are similar to the corresponding emissivity curves in figure C.4 (a)-(c) and the corresponding the photon emission coefficients (e.g. Balmer lines $n=3-6 \rightarrow 2$) shown in figure 5(a). Similarly, the curves of emissivity and Balmer photon emission coefficient via dissociation channel (H_2) and dissociative recombination channel (H_2^+) correspond to the rate coefficients of dissociation in figure C.2 and dissociative recombination in figure C.3,

respectively. For the mutual neutralization excitation channel (H^-), its emissivity curve is similar to the rate coefficient of reaction 7.2.3b ($H^+ + H^- \rightarrow H^+ + H + 2e$) in Amjuel [20].

Looking at the emissivity from hydrogen excited atoms at different energy levels ($n=2-6$), it can be seen that the deviation between the curves via direct electron-impact excitation is much larger than the one between the recombination emissions. Therefore, the intersection of emissivity for the two excitation channels is located at a larger T_e for a higher-n Lyman line. Once the electron density increases, the direct electron-impact excitation emissivity is slightly reduced, while the emissivity via electron-ion recombination emission increases. Thus, the emission via recombination channel tends to be more significant at higher densities. Moving now to molecular emission, in figure C.4(d)-(f), the emissivity variation between different Lyman lines is generally large for the three excitation channels considered. Only the emissivity of the Lyman line $n=3$ via H_2^+ and H^- does slightly decrease with increasing electron density, while the others change little. One thing should be noted for the molecular excitation channels: due to the small densities, the excitation via H_2^+ and H^- are less important at high temperatures, even though the emissivity via H_2^+ and H^- is greater than the other channels. They may become important in the divertor as their densities greatly enhance with the drop of temperature ($T_e < 3\text{eV}$) or with external fuelling (gas puffing). The photon emission via H_2^+ and H^- channel may also become important when $T_e < 3\text{eV}$, as the emission coefficients shown in figure C.5(b). In particular for H_{alpha} photon emission, H_2^+ and H^- are expected to be the dominant excitation channels.

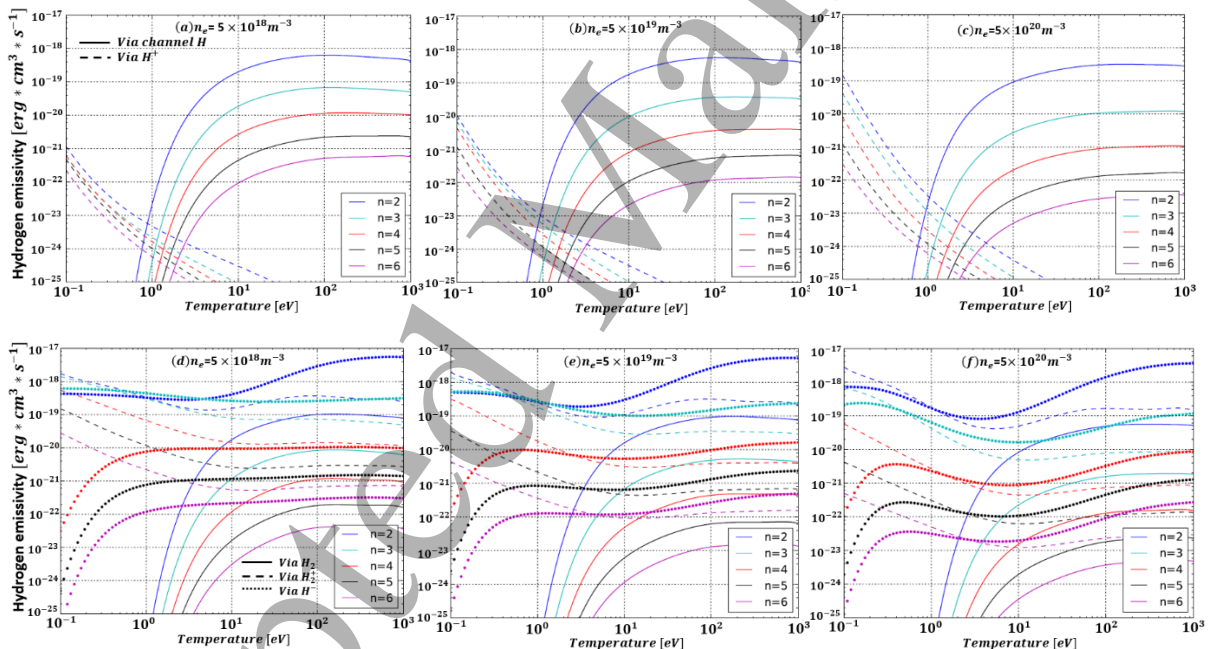


Figure C.4: Hydrogen emissivity of the hydrogen excited atom at different energy levels (Lyman lines $n=2-6 \rightarrow 1$) as a function of electron temperature for the electron density $n_e = 5 \times 10^{18} / \text{m}^3$, $n_e = 5 \times 10^{19} / \text{m}^3$ and $n_e = 5 \times 10^{20} / \text{m}^3$. Two atomic excitation channels (direct electron-impact excitation H and recombination H^+) and three molecular excitation channels (dissociation via H_2 , dissociative recombination via H_2^+ and mutual neutralization via H^-) are shown here.

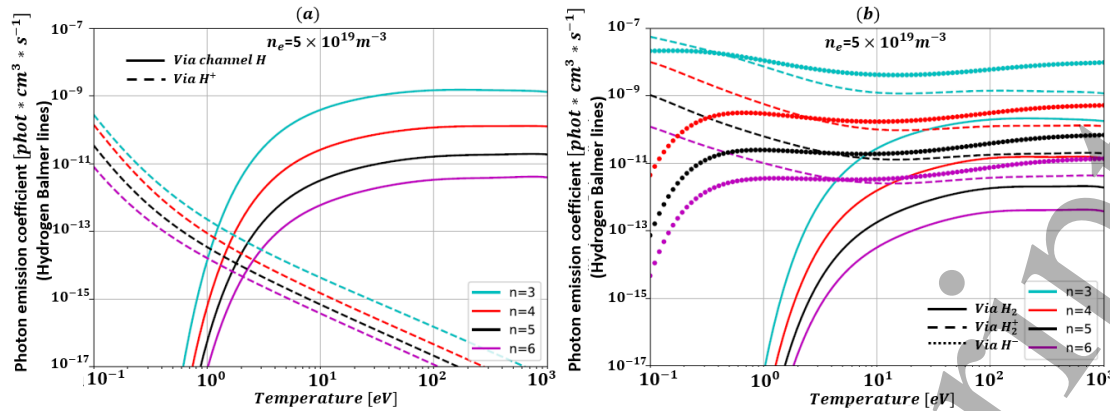


Figure C.5: Photon emission coefficient of the hydrogen excited atom at different energy levels (Balmer lines 3-6 → 2) as a function of electron temperature for the electron density $n_e = 5 \times 10^{19} / m^3$. (a) Two atomic excitation channels and (b) three molecular excitation channels are shown here.

This paper focuses on the study of divertor detachment in the hydrogen plasma conditions. But some other works have shown that the impact of isotope mass on neutral pressure, plasma density and other divertor conditions is crucial for divertor physics [32][33][34]. In deuterium or tritium operation, the peak electron density and neutral density might become higher in the divertor [32]. Divertor detachment is expected to be started at a higher target temperature and a lower upstream density [2][33]. In future work, we will investigate the effect of mass rescaling on divertor detachment.

D. A comparison of divertor detachment with and without hydrogen molecules

Investigating the behaviour of the particle flux Γ to the divertor target is a useful way to define the plasma detachment in both numerical and experimental research. We study here the rollover of Γ_{target} in all our scans, which include upstream density and upstream power flux. We compare the target particle flux to investigate the effects of molecules during detachment discharge with 1% carbon. All the simulations are implemented in MAST Upgrade like conditions: (1) the parallel heat flux is $50 MW/m^2$ at the X-point; (2) the connection length is 30m (20 m from X-point to target); (3) the effect of gradients in total magnetic field is considered with an area expansion factor (the ratio of $\frac{\text{Total field at X-point}}{\text{Total field at target}}$) of 2 between

X-point and target [16]. These are typical of expected Super-X divertor conditions in the first phase of MAST Upgrade operation [35]. 99% of plasma ion flux arriving at the target is recycled for all the cases considered. At the target, ions can recycle as both atoms or molecules, their relative ratio depending on the target material (and to a lesser extent, conditions). Here we include both recycling channels by changing such a ratio in a way that either atoms or molecules prevail. We have approached the problem by choosing three cases: one with just molecules as the recycling output, another with just atoms and a third with ions recycling as atoms or molecules with equal probability. The recycling temperature of neutral molecules and neutral atoms are $T_{H_2,recycle} = 0.1 eV$ (based on the temperature of the facing material) and $T_{H,recycle} = 3.5 eV$ (based on the Franck-Condon energy [17]) in our simulations.

We start with an upstream density scan for the cases without hydrogen molecules H_2 , as shown in figure D.1. Here we compare a case with and without carbon impurities. The results show that the plasma ion flux towards target rolls over at an upstream density $n_{up} \sim 1.8 \times 10^{19} / m^3$ for the case without carbon (labelled 'H'), while including 1% carbon (labelled 'H & carbon'), the rollover occurs at a lower n_{up} (about $1.69 \times 10^{19} / m^3$). Before the flux rollover, the influence of carbon impurity radiation is limited, but it gradually becomes significant after the rollover since both the plasma ion and carbon impurity

accumulate near target with the increase of n_{up} . Therefore, the carbon impurity radiation greatly increases in the cases with a higher n_{up} and leads to a lower target temperature.

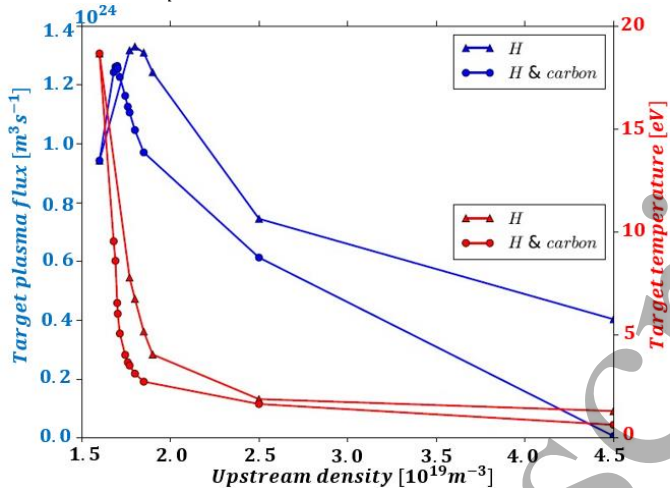


Figure D.1 Upstream density scan for the cases (a) without impurity and hydrogen molecule (labelled 'H'), (b) with 1% carbon impurity (labelled 'H & carbon')

In figure D.2 we investigate the impact of the recycling channel ($H^+ \rightarrow H$ and $H^+ \rightarrow H_2$) on the plasma flux roll-over and target temperature. When recycling releases hydrogen molecules H_2 in the simulation, it is found that the flux rollover occurs at a higher n_{up} (varied from $1.69 \times 10^{19}/m^3$ to $1.92 \times 10^{19}/m^3$) with a larger peak target flux, while the target temperatures before rollover gradually become higher. The reason is that the generation of hydrogen molecules from recycled ions reduces the atom source and density, therefore causing a lower electron-impact excitation radiation power loss and slowing the atom-plasma interactions, which are the main energy sinks before rollover in the divertor. In the case where the rollover occurs (e.g. the case at $n_{up} = 1.92 \times 10^{19}/m^3$ in figure D.2), the ratio of total amounts of molecule and atom ($\frac{\int n_m dV}{\int n_n dV}$) in the divertor could be up to 50% when all recycled plasma ions become molecules. As shown in figure D.3, the reduction of atom source from recycling can lead to a much smaller peak atom density near the target, such that the peak density of plasma ions near the target is also gradually reduced. The plasma-neutral collisional and radiative interactions are, therefore, mitigated. Furthermore, the density profiles of H^+ , H , H_2 and H_2^+ in figure D.3 indicate the plasma ion flux towards the target first interacts with neutral atoms and the ion density dramatically decreases before hitting the molecule cloud (H and H_2^+) near the target. Due to the lower plasma density and temperature near the target, the hydrogen radiation from excited atoms after molecular break-up involving (H_2 , H^- , H_2^+) is found to be much smaller than the electron-impact excitation radiation, which accounts for over 85% of hydrogen atom radiation power in the divertor. After the target ion flux rollover, which marks divertor detachment in figure D.2, the plasma ion flux reaching target starts dropping with increasing n_{up} . As the recycling flux is proportional to the target ion, molecule densities are found to quickly rise at the beginning of detachment and then slowly drop when the upstream density increases further and more atoms are produced by recombination (when $T_e < 1eV$) in the divertor. Hence, the molecule-plasma interactions might become less important than atom-plasma interactions once recombination becomes significant in the divertor. The details of the effects of different reaction types on plasma momentum loss are shown in figure D.7.

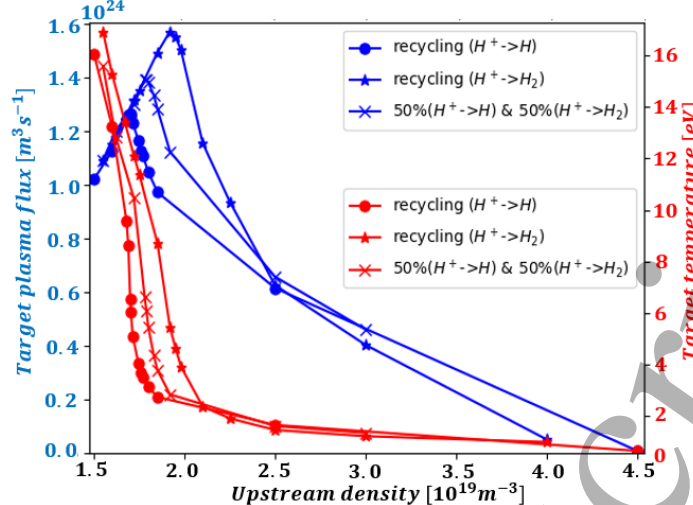


Figure D.2 Upstream density scan for the cases (a) with 1% carbon impurity and without molecules labelled 'recycling ($H^+ \rightarrow H$)', (b) with 1% carbon and hydrogen molecules (All recycled ions becomes molecules in this case), labelled 'recycling ($H^+ \rightarrow H_2$)', and (c) with 1% carbon and hydrogen molecules (half recycled ions becomes molecules and half becomes atoms in this case), labelled '50% ($H^+ \rightarrow H_2$) & 50% ($H^+ \rightarrow H$)'.

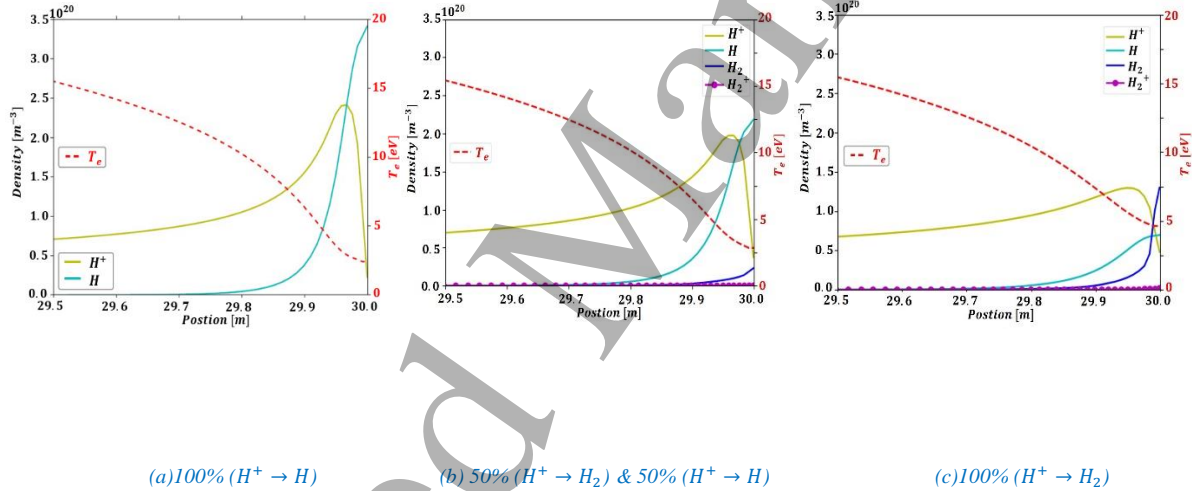


Figure D.3 Density profiles of H^+ , H , H_2 , H_2^+ and temperature profile of electron in the case with (a) all the recycled ions converting into atoms ($H^+ \rightarrow H$), (b) 50% recycled ions becoming atoms and the other half becoming molecules ('50% ($H^+ \rightarrow H_2$) & 50% ($H^+ \rightarrow H$)', and (c) all the recycled ions converting into molecules ($H^+ \rightarrow H_2$). The upstream density is $n_{up} = 1.92 \times 10^{19} / m^3$ for all the three cases, corresponding to the three cases at $n_{up} = 1.92 \times 10^{19} / m^3$ in figure D.2. The target is located at the position of 30m.

Our calculations also allow us to gain insight into the dissipation mechanisms at play. According to the Two Point Model (TPM) [2], the upstream and target static pressures should be such that $p_{up} = 2p_{target}$, if no momentum losses are considered. However, in the presence of plasma-neutral interactions, the plasma momentum will be affected and vary along the SOL. To keep into account this effect, a momentum loss factor is defined as:

$$f_m = 1 - 2p_{target}/p_{up} \quad (9)$$

Before the code upgrade, the studies with SD1D in the same MAST Upgrade like conditions [16], found that this momentum loss factor could be written as an exponent function:

$$\frac{2p_{target}}{p_{up}} = 1 - f_m = 0.9[1 - e^{(-\frac{T_{target}}{2.1})}]^{2.9} \quad (10)$$

According to the Self-Ewald model [16][36], the atom-ion charge exchange imposes a drag force on the plasma ion momentum, while ionisation produces plasma ions. This momentum loss mechanism is determined by ionisation and charge exchange, but it ignores many other factors, e.g. molecule-plasma interactions. The Self-Ewald model calculates the momentum loss factor as a function of ionisation and charge exchange rate coefficients [36]: $1 - f_m = [\frac{\alpha}{\alpha+1}]^{(\alpha+1)/2}$, where $\alpha = \langle \sigma v \rangle_{ion} / (\langle \sigma v \rangle_{ion} + \langle \sigma v \rangle_{cx})$. In the new version of SD1D used here, we calculate the momentum loss factor based on the direct interaction with the atomic and molecular species. As a consequence, we can plot $\frac{2p_{target}}{p_{up}}$ from the cases previously discussed in figure D.4, with the data well fitted by an exponential expression for the momentum loss factor (the black solid line):

$$\frac{2p_{target}}{p_{up}} = 1 - f_m = 0.889[1 - e^{(-\frac{T_{target}}{2.62})}]^{1.65}. \quad (11)$$

Having the target pressure from the expression above, we can now calculate the target particle flux: $\Gamma_{target} \propto n_{target} \sqrt{T_{target}} = p_{target} / \sqrt{T_{target}}$. Using the target pressure $p_{target} = \frac{(1-f_m)p_{up}}{2}$ from eq. 9, Γ_{target} can be written as:

$$\Gamma_{target} = p_{up} \frac{(1-f_m)}{\sqrt{8m_i T_{target}}} \quad (12)$$

A target temperature scan at fixed p_{up} for the target plasma flux is shown in figure D.5, which compares the simulations to the analytical calculations obtained by replacing our expressions for $(1 - f_m)$ into eq. 12. To complement figure D.2, it is interesting to visualize our results in a Γ_{target} versus target temperature plot, which is shown in figure D.5. What we see is that the detachment roll over occurs for all simulations at around 5eV regardless the specific recycling conditions. We could see that also eq. 12 together with the exponential expression in eq.11 give a curve for Γ_{target} that rolls over at a fixed target temperature as long as p_{up} does not vary much with the target temperature. To be more specific, we observe a small variation of the plasma temperature at rollover, with higher values (6.7eV) for recycling of pure atoms and smaller values (5.3eV) for pure molecular recycling.

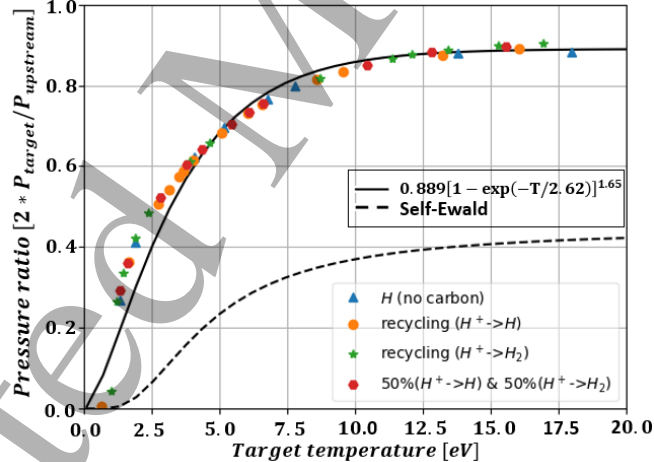


Figure D.4 Ratio of $\frac{2p_{target}}{p_{up}}$ as a function of target temperature achieved from the simulation cases without molecules (labelled 'H (no carbon)' and 'recycling ($H^+ \rightarrow H$)', with molecules introduced by different recycling conditions (labelled 'recycling ($H^+ \rightarrow H_2$)' and '50% ($H^+ \rightarrow H_2$) & 50% ($H^+ \rightarrow H$)')

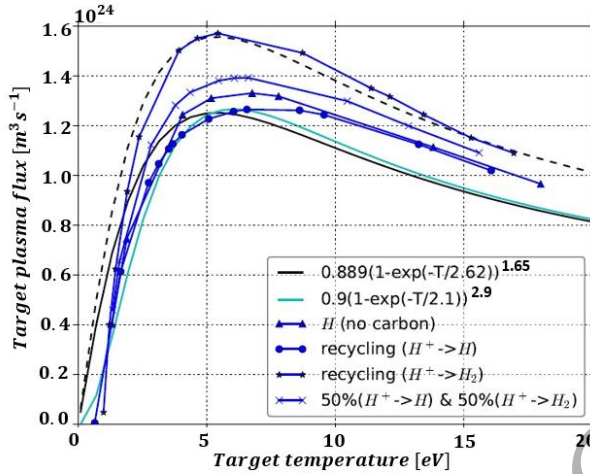


Figure D.5. Target flux as a function of target temperature for the upstream density scan in the cases: 1) without impurity and molecules labelled 'H (no carbon)', 2) with 1% carbon and without molecules labelled 'recycling ($H^+ \rightarrow H$)', 3) with 1% carbon and with hydrogen molecules labelled 'recycling ($H^+ \rightarrow H_2$)' and '50% ($H^+ \rightarrow H_2$) & 50% ($H^+ \rightarrow H$)'. The celeste and black solid curves show the target flux calculated with eq. 12 by using eq. 10 and eq. 11. The upstream density is $n_{up} = 1.97 \times 10^{19} / m^3$ for the black and celeste solid lines, while $n_{up} = 2.35 \times 10^{19} / m^3$ for the black dashed line.

Part of the the input power P_{in} is dissipated by the impurity radiation P_{imp} , part used to ionise the neutrals in the target region P_{ion} and the rest, P_{target} , reaches the target. According to [2], we define the power entering the recycling region

$$P_{rec} = P_{ion} + P_{target} = (E_{ion} + \gamma T_{target}) \Gamma_{target}, \quad (13)$$

where $\gamma T_{target} \Gamma_{target}$ represents the heat flux reaching the target and E_{ion} is the total effective ionisation energy (including hydrogen atomic radiation). Together with the eq.12, the detachment parameter $\frac{p_{up}}{P_{rec}}$ (p_{up} represents upstream pressure) could be obtained:

$$\frac{p_{up}}{P_{rec}} = \frac{\sqrt{8m_i T_{target}}}{(1-f_m)(E_{ion} + \gamma T_{target})} \quad (14)$$

$$= \frac{\sqrt{8m_i \gamma} E_{ion}^{-\frac{1}{2}} \left(\frac{\gamma T_t}{E_{ion}} \right)^{\frac{1}{2}}}{(1-f_m) \left(1 + \frac{\gamma T_t}{E_{ion}} \right)}$$

where $1 - f_m = \frac{2p_{target}}{p_{up}}$ is a function of target temperature as shown in eq.11. Thus, both the target temperature and the effective ionisation energy E_{ion} at the time when rollover occurs determine the detachment threshold $\frac{p_{up}}{P_{rec}}$. According to figure D.4, $1 - f_m$ varies little when $T_t > 10\text{eV}$, and steeply go to zero when $T_t < 10\text{eV}$. If a fixed ionisation energy is used in calculation, $\frac{p_{up}}{P_{rec}}$ grows as the target temperature decreases (dashed line in figure D.6). We can absorb the effect of neutral radiation in the ionization energy in an ad hoc way, which is an approximation that is sometimes used to capture both effects. If we do so, E_{ion} becomes a function of the target temperature, which now would represent the total energy loss of ionisation plus hydrogen atom excitation divided by the ionisation rate. This assumes that all ionisation occurs directly at the target (e.g. occurs at a target temperature T_t). We have shown this quantity as a red solid line in figure D.6, by using our numerical results from the simulation with pure molecular recycling. We have found that the other simulations with different recycling conditions produced similar results. Using this in (14), we find that the ratio of $\frac{p_{up}}{P_{rec}}$ is about $9.5N/MW$ at high temperatures, and it quickly decreases when $T_t < 10\text{eV}$, as the blue solid line shows in figure D.6. Generally, the target flux rollover, indicating onset of detachment, occurs when a critical value of the gradient of E_{ion} with respect to T_t is achieved [2][16][27]:

$$\frac{\partial E_{ion}}{\partial T_t} < -\gamma, \quad (15)$$

For the sheath transmission coefficient γ used in this paper ($\gamma = 6$), we find $T_t = 5.6\text{eV}$ and the corresponding effective ionisation energy $E_{ion} = 82.23\text{eV}$. This corresponds to the value of the detachment parameter given below:

$$\frac{p_{up}}{P_{rect}} = 8.1 \text{ N/MW},$$

which is smaller than 12.6N/MW found in the old SD1D [16] and 17N/MW found in SOLPS4.3 simulation on DIII-D like equilibria [37]. The different results obtained in the upgraded SD1D and the previous version are very likely due to different effective ionisation energy ($E_{ion} = 60.8\text{eV}$ in the previous version). Variations in this quantity with model assumptions and inputs are expected: The ratio $\frac{p_{up}}{P_{rect}}$ is not a universal quantity though it has a physical basis. This quantity is however experimentally measurable, and is an important metric that can be used for comparisons between simulation and experiments.

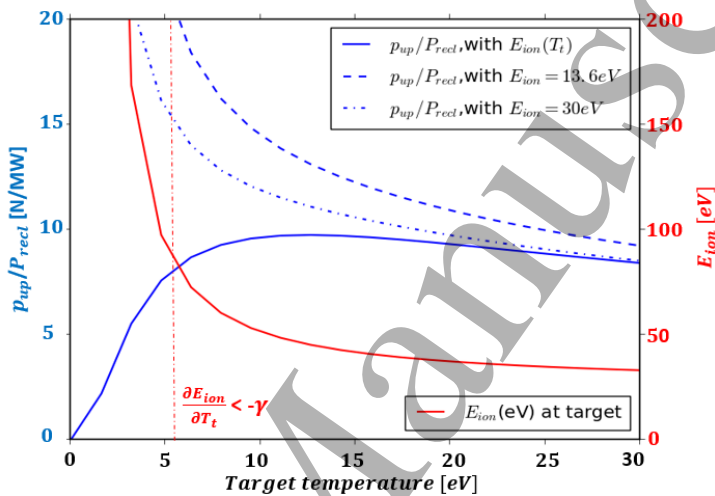


Figure D.6. $\frac{p_{up}}{P_{rect}}$ as a function (eq.14) of target temperature and effective ionisation energy E_{ion} . $\frac{p_{up}}{P_{rect}}$ is calculated with fixed $E_{ion} = 13.6\text{eV}, 30\text{eV}$ and with the $E_{ion}(T_t)$ as a function of target temperature (which is the total energy loss of ionisation and hydrogen atom emission divided by the ionisation rate as the red solid line shows). The threshold in eq.15 is marked by the vertical red dashed line.

As discussed in some previous works [11][27], plasma ions can undergo charge exchange collisions with hydrogen molecules ($H^+ + H_2 \rightarrow H_2^+ + H$) in the divertor, which may account for a rise of plasma ion momentum loss in the low temperature region. To investigate the importance of molecule-plasma charge exchange and other reaction types, we use a momentum loss factor $f_{momloss} = (\sum_p \int_{up}^{target} F_{H^+ - p} dl) / p_{up}$, where $\sum_p \int_{up}^{target} F_{H^+ - p} dl$ is the total energy loss of H^+ by the collisions with other particle species ‘p’ ($F_{H^+ - p}$ represents collision force). Based on SD1D simulations (the case of ‘recycling ($H^+ \rightarrow H_2$)’), we found molecule density near the target increases quickly at the onset of detachment ($n_{H_2} > n_H$ at this moment), and thus it is found that in figure D.7(a) the momentum loss $f_{momloss}$ caused by $H_2 - H^+$ rises rapidly and is more important than other collisions when $n_{up} < 2.2 \times 10^{19}/\text{m}^3$. But with the n_{up} growing further, the growth of molecule density becomes slower and the peak molecule density is even found to decrease at high upstream densities ($n_{up} > 3.5 \times 10^{19}/\text{m}^3$) due to the decreasing recycling source (plasma ion flux at the target Γ_{target}) and no external fuelling included. As a result, $H_2 - H^+$ collisions becomes less important, while $H - H^+$ collisions provide the largest part of momentum loss because recombination produces more neutral atoms at low temperatures ($n_{H_2} < n_H$ at this moment). In figure D.7(b), it compares the momentum loss caused by two main $H_2 - H^+$ interactions, charge exchange and elastic collision. The simulation results predict that the momentum loss mechanism via $H_2 - H^+$ interactions is primarily due to $H_2 - H^+$ elastic collisions, instead of ion-molecular charge exchange.

H_{alpha} emission is crucial for tokamak experiment diagnostics, and conveys information on neutral density and neutral-plasma interactions. The upgraded SD1D model includes the main H_{alpha} emission processes, including the H_{alpha} emission from direct electron-impact excitation and from excited atoms generated via electron-ion recombination and plasma-molecule interactions. Therefore, it is able to investigate the total H_{alpha} emission and the importance of different excitation channels. In figure D.7(c), simulations found that atomic channels (primarily direct electron-impact excitation) dominate H_{alpha} emission before Γ_{target} rollover and then change little during detachment, while molecular channels account for the strong rise of H_{alpha} signal, which grows to be 5 times the H_{alpha} emission at Γ_{target} rollover ($n_{up} = 1.92 \times 10^{19}/m^3$). This is mainly due to the fast growth of molecule density near the target at the beginning of detachment and then due to the increase of H_{alpha} emission coefficients via dissociative excitation ' H_2^+ ', and mutual neutralization ' H^- ' (figure C.5(b)) with the decrease of T_e when $T_e < 3.0\text{eV}$. This result well matches the measured and predicted photon emission on TCV [38]. Further analysis of the decomposition of molecular channels in figure D.7(d) shows the rise of H_{alpha} signal is firstly due to H_2^+ channel ($1.92 \times 10^{19}/m^3 < n_{up} < 2.5 \times 10^{19}/m^3$) and then H^- channel becomes more important when the target gets further detached ($n_{up} > 2.5 \times 10^{19}/m^3$).

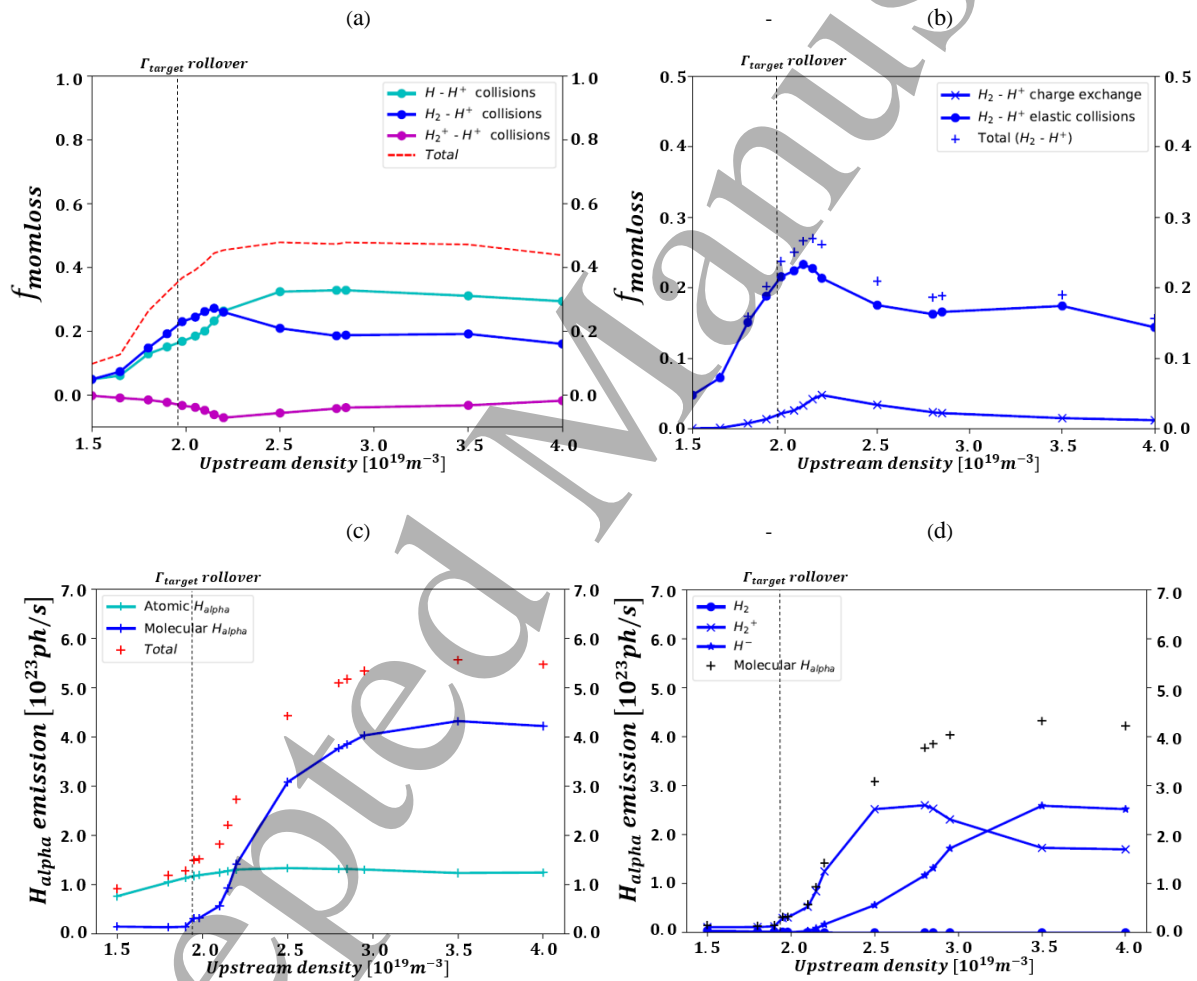


Figure D.7 (a) Decomposition of momentum loss factor $f_{momloss}$ due to different reaction types, labelled as ' $H - H^+$ ', ' $H_2 - H^+$ ', ' $H_2^+ - H^+$ ' collisions, and their total $f_{momloss}$ (the red dashd) when all recycled ions become molecules; (b) Decomposition of $f_{momloss}$ caused by $H_2 - H^+$ collisions.(c) decomposition of total H_{alpha} photon emission due to atomic and molecular channel, (d) decomposition of H_{alpha} photon emission through molecular channels. Vertical dashed lines indicates the position of Γ_{target} rollover.

5 E. Conclusions

In the previous version of SD1D, only atomic collisional and radiative reactions were included, while molecular processes were only indirectly included as part of effective reaction and emission rates. To better investigate the physics of divertor detachment, an important upgrade has been carried out of the SD1D model by adding a molecule model, including hydrogen molecule H_2 and charged molecule H_2^+ species. The Amjuel database [20] is now used to provide data of the molecular collisional and radiative reactions listed in Table 1.

Using the upgraded SD1D code in MAST Upgrade like conditions, we have studied the role of H_2 and H_2^+ in detached regimes of tokamak plasmas. It is found that molecules play an important role in the flux rollover, which occurs at a higher upstream density and a slightly lower target temperature if a larger proportion of H_2 generated from recycling process.

Generally the target flux rollover, indicating onset of detachment, occurs when a critical value of the gradient of E_{ion} with respect to T_{target} is achieved: $\frac{\partial E_{ion}}{\partial T_t} < -\gamma$ [2][16]. For the sheath transmission coefficient $\gamma = 6$ used in this paper, we find $T_t = 5.6\text{eV}$ and the corresponding effective ionisation energy $E_{ion} = 82.23\text{eV}$ for flux rollover. In the simulations, we also calculated the momentum loss factor $f_m = 1 - 2p_{target}/p_{up}$ and obtained $\frac{2p_{target}}{p_{up}}$ as a function of target temperature: $\frac{2p_{target}}{p_{up}} = 1 - \frac{f_m}{0.889[1 - e^{(-\frac{T_{target}}{2.62})}]}^{1.65}$. This corresponds to the value of the critical detachment parameter (eq. 14) given as $\frac{p_{up}}{p_{recl}} = 8.1 \text{ N/MW}$, which is smaller than the value found by the previous version of SD1D [16].

The SD1D simulations predict that both molecule-plasma and atom-plasma collisions can lead to a large plasma momentum loss during detachment. The decomposition of momentum loss shows molecule-plasma elastic collision dominates molecule-plasma interactions, while molecular charge exchange cannot effectively reduce plasma momentum. H_{alpha} emission is also considered in SD1D simulations, which found a strong rise of H_{alpha} signal when the upstream density is increased after rollover. The H_2^+ channel accounts for the most growth of H_{alpha} at the onset of detachment and then the H^- channel contributes more when the target becomes further detached.

SD1D has wide applicability, and is able to simulate divertor detachment on other devices, e.g. DIII-D, TCV and ITER. In future studies, it will be interesting to investigate the effects of molecular species on divertor detachment on other devices.

42 F. Appendix

43 1. The definition of sources and sinks

44 The source and sink terms in density equation(S), momentum equation(F) and energy
45 equation(E and R) caused by the collisional reactions shown in table 1 are defined as below:

51 Ionisation:

52 $S_H^{ion} = -S_{H^+}^{ion} = n_H n_e \langle \sigma v \rangle_{ion}$, $F_H^{ion} = -F_{H^+}^{ion} = m_H V_H n_H n_e \langle \sigma v \rangle_{ion}$, $E_H^{ion} = -E_{H^+}^{ion} =$
53 $\frac{3}{2} T_H n_H n_e \langle \sigma v \rangle_{ion}$ and $R_e^{ion} = 13.6\text{eV} \times n_H n_e \langle \sigma v \rangle_{ion}$;

55 Electron-ion Recombination:

56 $S_{H^+}^{rec} = -S_H^{rec} = n_{H^+} n_e \langle \sigma v \rangle_{rec}$, $F_{H^+}^{rec} = -F_H^{rec} = m_{H^+} V_{H^+} n_{H^+} n_e \langle \sigma v \rangle_{rec}$ and $E_{H^+}^{rec} =$
57 $-E_H^{rec} = \frac{3}{2} T_{H^+} n_{H^+} n_e \langle \sigma v \rangle_{rec}$;

59 Charge exchange (CX):

1
2
3 $F_{H^+}^{CX} = -F_H^{CX} = n_{H^+}n_H < \sigma v >_{CX} m_{H^+}(V_{H^+} - V_H)$ and $E_{H^+}^{CX} = -E_H^{CX} = n_{H^+}n_H <$
4 $\sigma v >_{CX} \frac{3}{2}(T_{H^+} - T_H)$;
5
6

7 **Non-dissociative ionisation:**

8 $S_{H_2}^{ion} = -S_{H_2^+}^{ion} = n_{H_2}n_e < \sigma v >_{ion}^{H_2}$, $F_{H_2}^{ion} = -F_{H_2^+}^{ion} = m_{H_2}V_{H_2}n_{H_2}n_e < \sigma v >_{ion}^{H_2}$ and $E_{H_2}^{ion} =$
9 $-E_{H_2^+}^{ion} = \frac{3}{2}T_{H_2}n_{H_2}n_e < \sigma v >_{ion}^{H_2}$;

10 **Dissociation:**

11 $S_{H_2}^{diss} = -0.5 \times S_H^{diss} = n_{H_2}n_e < \sigma v >_{diss}^{H_2}$, $F_{H_2}^{diss} = -F_H^{diss} = m_{H_2}V_{H_2}n_{H_2}n_e < \sigma v >_{diss}^{H_2}$,
12 $E_{H_2}^{diss} = -E_H^{diss} = \frac{3}{2}T_{H_2}n_{H_2}n_e < \sigma v >_{diss}^{H_2}$ and $R_e^{diss} = 4.25eV \times n_{H_2}n_e < \sigma v >_{diss}^{H_2}$, where
13 4.25eV is the bind energy of a hydrogen molecule;

14 **Molecular charge exchange:**

15 The momentum and energy of H_2 transfer to H_2^+ , while the momentum and energy of H^+
16 transfer to H .

17 $S_{H_2}^{CX} = S_{H^+}^{CX} = -S_{H_2^+}^{CX} = -S_H^{CX} = n_{H_2}n_{H^+} < \sigma v >_{CX}^{H_2}$

18 $F_{H_2}^{CX} = -F_{H_2^+}^{CX} = m_{H_2}V_{H_2}n_{H_2}n_{H^+} < \sigma v >_{CX}^{H_2}$

19 $F_{H^+}^{CX} = -F_H^{CX} = m_{H^+}V_{H^+}n_{H_2}n_{H^+} < \sigma v >_{CX}^{H_2}$

20 $E_{H^+}^{CX} = -E_H^{CX} = \frac{3}{2}T_{H^+}n_{H_2}n_{H^+} < \sigma v >_{CX}^{H_2}$

21 $E_{H_2}^{CX} = -E_{H_2^+}^{CX} = \frac{3}{2}T_{H_2}n_{H_2}n_{H^+} < \sigma v >_{CX}^{H_2}$

22 **Dissociative excitation (DE):**

23 $S_{H_2^+}^{DE} = -S_{H^+}^{DE} = -S_H^{DE} = n_{H_2^+}n_e < \sigma v >_{DE}^{H_2^+}$, $F_{H_2^+}^{DE} = -2 \times F_{H^+}^{DE} = -2 \times F_H^{DE} =$
24 $m_{H_2^+}V_{H_2^+}n_{H_2^+}n_e < \sigma v >_{DE}^{H_2^+}$ and $E_{H_2^+}^{DE} = -2 \times E_{H^+}^{DE} = -2 \times E_H^{DE} = \frac{3}{2}T_{H_2^+}n_{H_2^+}n_e <$
25 $\sigma v >_{DE}^{H_2^+}$;

26 **Dissociative ionisation (DI):**

27 $S_{H_2^+}^{DI} = -0.5 \times S_{H^+}^{DI} = n_{H_2^+}n_e < \sigma v >_{DI}^{H_2^+}$, $F_{H_2^+}^{DI} = -F_{H^+}^{DI} = m_{H_2^+}V_{H_2^+}n_{H_2^+}n_e < \sigma v >_{DI}^{H_2^+}$
28 and $E_{H_2^+}^{DI} = -E_{H^+}^{DI} = \frac{3}{2}T_{H_2^+}n_{H_2^+}n_e < \sigma v >_{DI}^{H_2^+}$;

29 **Dissociative recombination (DR):**

30 $S_{H_2^+}^{DR} = -0.5 \times S_H^{DR} = n_{H_2^+}n_e < \sigma v >_{DR}^{H_2^+}$, $F_{H_2^+}^{DR} = -F_H^{DR} = m_{H_2^+}V_{H_2^+}n_{H_2^+}n_e < \sigma v >_{DR}^{H_2^+}$
31 and $E_{H_2^+}^{DR} = -E_H^{DR} = \frac{3}{2}T_{H_2^+}n_{H_2^+}n_e < \sigma v >_{DR}^{H_2^+}$;

32 **Molecular activated recombination (MAR) via H^- :**

33 $S_{H_2}^{MAR} = S_{H^+}^{MAR} = -\frac{1}{3}S_H^{MAR} = n_{H_2}n_e < \sigma v >_{MAR}^{H_2}$

34 $F_{H_2}^{MAR} = m_{H_2}V_{H_2}n_{H_2}n_e < \sigma v >_{MAR}^{H_2}$

35 $F_{H^+}^{MAR} = m_{H^+}V_{H^+}n_{H_2}n_e < \sigma v >_{MAR}^{H_2}$

36 $F_H^{MAR} = -m_{H_2}V_{H_2}n_{H_2}n_e < \sigma v >_{MAR}^{H_2} - m_{H^+}V_{H^+}n_{H_2}n_e < \sigma v >_{MAR}^{H_2}$

37 $E_{H_2}^{MAR} = \frac{3}{2}T_{H_2}n_{H_2}n_e < \sigma v >_{MAR}^{H_2}$

38 $E_{H^+}^{MAR} = \frac{3}{2}T_{H^+}n_{H_2}n_e < \sigma v >_{MAR}^{H_2}$

39 $E_H^{MAR} = -E_{H_2}^{MAR} - E_{H^+}^{MAR} = -\frac{3}{2}T_{H_2}n_{H_2}n_e < \sigma v >_{MAR}^{H_2} - \frac{3}{2}T_{H^+}n_{H_2}n_e < \sigma v >_{MAR}^{H_2}$.

The energy sink of plasma caused by hydrogen excitation radiation is given by eq.8 in section B.2.

2. The rate coefficients in Hydhel databases

Figure F.1 shows the rate coefficients calculated by using Hydhel databases [31], which is a collection of reaction cross-sections and rate coefficients for hydrogen-helium plasmas. As mentioned in section C-1, the main difference is that the rate coefficients of Hydhel do not depend on electron density, while rate coefficients depend on both electron temperature and plasma density. An error will inevitably appear if the Hydhel database is applied to study divertor physics, particular detachment where the range of plasma density can be large. With the increase of electron density in figure C.1, specifically, the rate coefficient greatly enhances at lower temperatures (e.g. $T_e < 5\text{eV}$), while no such change occurs in figure F.1(a). Thus, it may contribute a significant error to the hydrogen atom and plasma ion densities. Another crucial difference is that the rate coefficients of molecular charge exchange and dissociation in figure F.1(b) are about 1 order smaller than the results shown in figure C.2 at $T_e < 10\text{eV}$. It will largely reduce the molecule sink in simulations, and therefore narrows the source of charged molecule H_2^+ . The dissociative excitation rate coefficient from Amjuel includes the component $e + H_2^+ \rightarrow H^* + H \rightarrow H^+ + H$, while the dissociative excitation rate coefficient from Hydhel consider $e + H_2^+ \rightarrow e + H_2^{+*} \rightarrow H^+ + H$ [20] [31]. H^* and H_2^{+*} represent the excited atom and vibrational excited molecule. As discussed in section C-2, H_2 and H_2^+ just convert into the excited atom in this paper. Thus, the Amjuel database is applied to provide dissociative excitation rate coefficient in simulations.

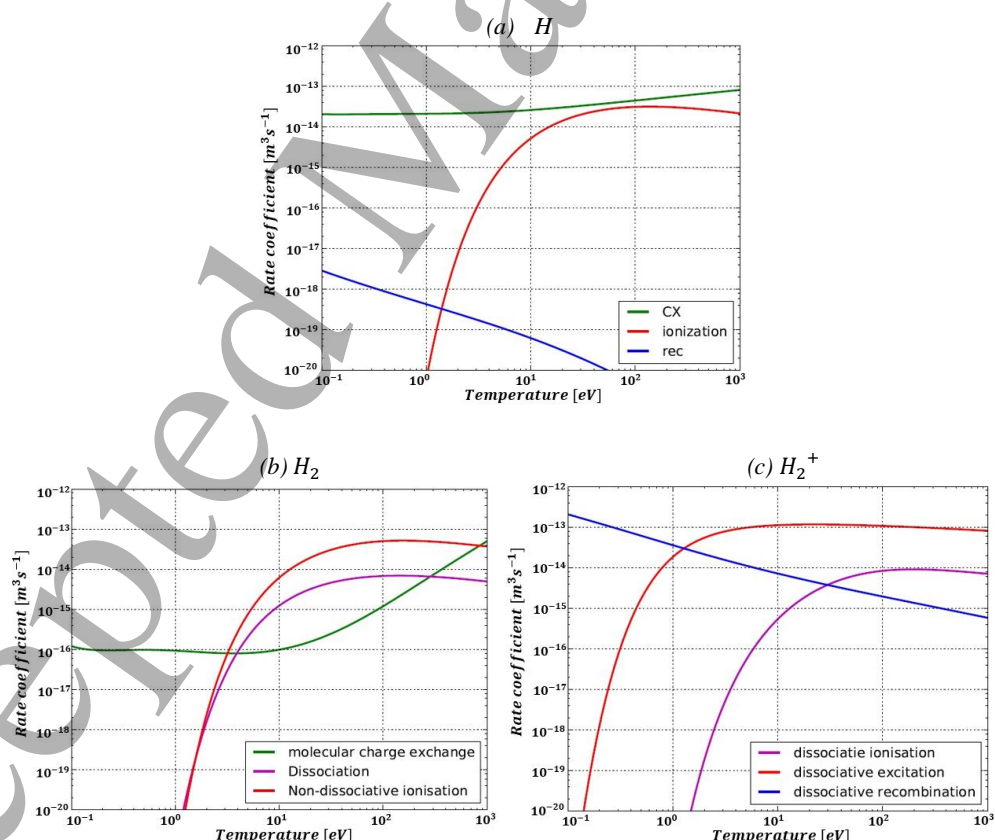


Figure F.1 The rate coefficients of collisional reactions related to (a) hydrogen atom H , (b) molecule H_2 and (c) charged molecule H_2^+ , calculated by data from [31]

G. Data availability statement

The data that support the findings of this study are available upon reasonable request from the authors.

H. Acknowledgements

This work has been (part-) funded by the National Science Foundation for Young Scientists of China (Grant No. 11805055), the RCUK Energy Programme [grant number EP/T012250/1], the U.S. DoE by LLNL under Contract DE-AC52-07NA27344, the China Scholarship Council (award to Yulin Zhou for a 3 year PhD programme at University of York), the Chinese ITER Project (2018YFE0303102) and CFETR project (2017YFE0302100). To obtain further information on the data and models underlying this paper please contact vz3138@york.ac.uk

I. References

- [1]. A. Kallenbach, M. Bernert, R. Dux, F. Reimold, M. Wischmeier, and ASDEX Upgrade Team. Plasma Physics and Controlled Fusion, [58\(4\):045013, 2016](#)
- [2]. P. C. Stangeby, Plasma Physics and Controlled Fusion, [60\(4\):044022, 2018](#)
- [3]. H. J. Kunze, Introduction to plasma spectroscopy, [volume 56. Springer](#), 2009
- [4]. M. Bernert, M. Wischmeier, A. Huber, F. Reimold, B. Lipschultz, C. Lowry, S. Brezinsek, R. Dux, T. Eich, A. Kallenbach et al., Nuclear Materials and Energy, [12:111-118, 2017](#)
- [5]. S. I. Krasheninnikov, A. Yu. Pigarov and D. J. Sigmar. Physics Letters A, [214, 285 \(1996\)](#)
- [6]. S. I. Krasheninnikov, A. S. Kukushkin, and A. A. Pshenov, Phys. Plasmas, [23\(5\):055602, 2016](#)
- [7]. D. Moulton, J. Harrison, B. Lipschultz, and D. Coster, Plasma Physics and Controlled Fusion, [59\(6\):065011, 2017](#)
- [8]. I. Paradela Pérez, A. Scarabosio, M. Groth, M. Wischmeier, F. Reimold, and ASDEX Upgrade Team. Nuclear Materials and Energy, [12:181-186, 2017](#)
- [9]. I Bykov, D L Rudakov, A Yu Pigarov et al., Phys. Scr. [T171 \(2020\) 014058](#)
- [10].C. Zhang, C. F. Sang, L. Wang et al., Plasma Phys. Control. Fusion [61 \(2019\) 115013](#)
- [11].K. Verhaegh, B. Lipschultz, J.R. Harrison, B.P. Duval et.al., [Nucl. Fusion 61\(2021\) 106014](#)
- [12].H. L. Du, C. F. Sang, L. Wang, X. Bonnin, H. Y. Guo, J. Z. Sun and D. Z. Wang, [Plasma Phys. Control. Fusion](#) 58 085006, 2016
- [13].M. Groth, E. M. Hollmann, A. E.Jaervinen et al, Nuclear Materials and Energy [19:211-217, 2019](#)
- [14].H. Bufferand, G. Ciraolo, Y. Marandet, J. Bucalossi, Ph. Ghendrih, J. Gunn, N. Mellet, P. Tamain et al [Nucl. Fusion 55:053025 \(2015\)](#)
- [15].S. I. Krasheninnikov and A. S. Kukushkin, J. Plasma Phys., [83:155830501, 2017.](#)
- [16].B. Dudson, J. Allen, T. Body, B. Chapman, C. Lau, L. Townley, D. Moulton, J. Harrison and B. Lipschultz, [Plasma Phys. Control. Fusion 61 \(2019\) 065008](#)
- [17].M. Nakamura, S. Togo, M. Ito and Y. Ogawa, J. Plasma Fusion Res., [6:2403098, 2011](#)
- [18].S. Togo et al. J. Plasma Fusion Res., [8:2403096, 2013](#)
- [19].E Havlíčková, W Fundamenski, V Naulin, A H Nielsen, R Zagórski, J Seidl and J Horáček, Plasma Phys. Control. Fusion [53:065004 \(2011\)](#)
- [20].D. Reiter, The data file AMJUEL: Additional Atomic and Molecular Data for EIRENE, [Version: January 13, 2020](#)
- [21].T. Body, 'Simulating Radiative Cooling and Detachment in a Divertor Plasma', thesis submitted for degree of MSc, University of York 2017
- [22].H. P. Summers. The ADAS user manual, version 2.6, 2004.
- [23].E. Havlíčková, W. Fundamenski, F. Subba, D. Coster, M. Wischmeier and G. Fishpool, Plasma Phys. Control. Fusion, [55 065004, 2013](#)
- [24].J. Leddy, B. Dudson and H. Willett, Nuclear Materials and Energy, [12:994-998,2017](#)
- [25].D. Wunderlich and U. Fantz. [Atoms, 4\(4\), 2016](#)
- [26].NIST Standard Reference Database 78, Version 5.7, 2019. URL: <https://dx.doi.org/10.18434/T4W30F>
- [27].K. Verhaegh, B Lipschultz, C Bowman, B P Duval et.al, Plasma Phys. Control. Fusion, [63\(2021\) 035018](#)

1
2
3 [28]. V. Kotov, D. Reiter, A. S. Kukushkin, *Numerical study of the ITER divertor plasma with the B2-EIRENE code package*, Technical report, Forschungszentrums Juelich (Germany), [Nov 2007: 142 p](#)
4
5 [29]. Y.P. Chen, D.R. Zhang, S.C. Liu, G.S. Xu, L. Wang, D.M. Yao, Z.P. Luo, L.Q. Hu and EAST Team, Nucl. Fusion, 60: 036019 2020, URL: <https://doi.org/10.1088/1741-4326/ab69e3>
6
7 [30]. H. Frerichsa, X. Bonnin, Y. Feng, A. Loarte, R. A. Pitts, D. Reiter, O. Schmitz, Nuclear Materials and Energy, [18: 62-66, 2019](#)
8
9 [31]. R. K. Janev, D. Reiter, U. Samm, Collision Processes in Low-Temperature Hydrogen Plasmas, [Forschungszentrum, Zentralbibliothek Jülich 2003](#)
10
11 [32]. J. Ulljanovs, M. Groth, A. E. Jaervinen, D. Moulton et al, Nuclear Material and Energy, [12: 791-797, 2017](#)
12
13 [33]. V. Solokha, M. Groth, S. Brezinsek, M. Brix, G. Gorriagan et al, Nuclear Material and Energy, [25: 100836, 2020](#)
14
15 [34]. C. F. Maggi, R. D. Monk, L. D. Horton, K. Borrass et al, Nuclear Fusion, [39: 979, 1999](#)
16
17 [35]. E. Havlíčková, W. Fundamenski, M. Wischmeier, G. Fishpool and A. W. Morris, Plasma Phys. Control. Fusion [56\(2014\) 075008](#)
18
19 [36]. S. A. Self and H. N. Ewald, Physics of Fluids, [09: 2486, 1966](#).
20
21 [37]. A. A. Pshenova, A. S. Kukushkina and S. I. Krasheninnikov, Nuclear Materials and Energy, [12: 948-952, 2017](#)
22
23 [38]. K. Verhaegh, B. Lipschultz, J.R. Harrison, B.P. Duval et.al., Nuclear Materials and Energy, [26 \(2021\) 100922](#)
24
25
26
27
28
29
30
31
32
33
34
35
36
37
38
39
40
41
42
43
44
45
46
47
48
49
50
51
52
53
54
55
56
57
58
59
60